JMEPEG (2024) 33:9716–9731
https://doi.org/10.1007/s11665-023-08603-z

1059-9495/$19.00

ORIGINAL RESEARCH ARTICLE

Influence of Plasma Immersion Ion Implantation on Ti-6Al-4V Alloy Tensile–Tensile Fatigue Behavior: The Introduction of Shot Peening as a Pretreatment

V.M.C.A. Oliveira, L. Nozaki, M.F. Fernandes, M.O.H. Cioffi, R. Oliveira, L.G. Martinez, M.J.R. Barboza, and H.J.C. Voorwald

Submitted: 29 March 2023 / Revised: 28 June 2023 / Accepted: 29 July 2023 / Published online: 21 August 2023

The purpose of this study was to investigate the influence of combined plasma immersion ion implantation (PIII) and shot peening (SP) treatments on the axial fatigue strength of the Ti-6Al-4V alloy. The specimens were superficially treated with SP and PIII separately and in a combined way. The tensile–tensile fatigue behavior was investigated based on microstructural analysis, residual stress measurements, profilometry, Vickers microhardness, scanning electron microscopy, and transmission electron microscopy. Axial fatigue tests at room temperature were performed for the Ti-6Al-4V base material, PIII at 500 and 800 °C, SP process and the combination of both surface treatments. The residual stress measurements indicated that PIII treatment at 500 °C induced tensile residual stresses of 189 MPa on the material surface. The PIII treatment at 500 °C maintained the fatigue resistance of the Ti-6Al-4V alloy in the low-cycle fatigue region, while the PIII treatment at 800 °C reduced the fatigue life at all stress levels, from 32 to 96% reduction in lifetime. The combination of SP pretreatment and PIII treatment at 500 °C decreased the tensile residual stress value at the surface from 189 to 23 MPa, resulting in an improvement of the fatigue strength compared to only PIII treatment, for $N = 10^6$, the fatigue strength doubled in value. The analysis and tests presented in this work showed the potential of combining PIII and SP treatments to promote the surface protection without the substantial fatigue strength loss frequently associated to surface treatments.

Keywords fatigue, plasma immersion ion implantation, residual stress, shot peening, Ti-6Al-4V alloy

1. Introduction

Titanium alloys are widely applied in the aeronautical industry due to high mechanical strength to weight ratio and high corrosion resistance (Ref 1-3). The microstructure of Ti-6Al-4V alloy is sensitive to heat treatment and can be modified by the cooling rate to achieve a desirable combination of properties. The most common morphologies are equiaxed (with α equiaxed grains surrounded by β phase at grain boundaries), lamellar (with α and β lamellae phases arranged alternatingly and with different crystallographic orientations), and bimodal (microstructure having α grains and grains with α and β phases arranged in lamellar form). All these morphologies have been described in the literature and presented good impact toughness, comprehensive properties, and creep resistance (Ref 4-7). However, titanium alloys also present low machinability, thermal conductivity, high chemical reactivity, and a high friction coefficient (Ref 8, 9). Therefore, surface treatments are frequently applied to Ti-6Al-4V alloy, to improve tribological properties.

The deposition of coatings, to improve corrosion and tribological properties, is frequently associated with a substantial fatigue life reduction due to the brittle coating deposition, defects in the film, microcracks, and tensile residual stresses. However, surface treatments can also improve the fatigue strength of Ti-6Al-4V alloy by delaying crack nucleation, reducing the crack propagation rate, modifying mechanical properties, altering chemical compositions, and inducing compressive residual stresses on surfaces (Ref 10).

Plasma immersion ion implantation (PIII) is a potential surface treatment alternative via the implantation of interstitial high-energy ions accelerated toward the target, which is negatively charged. The impact introduces these interstitial ions (typically nitrogen) into the surface, which is modified by either solid solution hardening or ceramic coating formation (which is a product of metal and ion reactions). Ion implantation can penetrate a maximum of a few tens of micrometers from the surface (Ref 11). PIII can be applied to improve hardness, corrosion, and wear properties (Ref 12-14), and presented a lower influence on fatigue strength loss than the others deposition techniques (Ref 15).

Shot peening (SP) can be applied to recover part of the fatigue life loss after surface treatments. The process consists of impacting the surface to generate compressive residual stresses,

V.M.C.A. Oliveira, L. Nozaki, M.F. Fernandes, M.O.H. Cioffi, and **H.J.C. Voorwald**, Department of Materials and Technology, Fatigue and Aeronautic Materials Research Group, School of Engineering, São Paulo State University (UNESP), Guaratinguetá, Brazil; **R. Oliveira**, Associated Laboratory of Plasmas, Instituto Nacional de Pesquisas Especiais – INPE, São José dos Campos, Brazil; **L.G. Martinez**, Crystallography Laboratory Applied to Materials Science, Instituto de Pesquisas Energéticas e Nucleares – IPEN, São Paulo, Brazil; **M.J.R. Barboza**, Department of Materials, Escola de Engenharia de Lorena, Universidade de São Paulo – USP, Lorena, Brazil. Contact e-mail: veronicamcaoliveira@gmail.com.

grain refinement, work hardening, and improve mechanical strength (Ref 15). Wang and collaborators (Ref 16) studied the effect of shot peening and laser shock peening treatments combination on the Ti6Al4V fatigue strength. For this purpose, the authors studied the effects of the separate treatments on the microstructure and mechanical properties of the alloy and compared them with the effects of the combined treatments, and with the untreated Ti6Al4V alloy. Regarding the effects of the SP treatment, alone, compared to the properties of the untreated alloy, the authors reported: hardness increase of 5.6%; layer depth affected by shot peening of 200 μm; and increase of fatigue resistance, in a high cycle regime. Furthermore, the authors concluded that, as the SP treatment can introduce a higher plastic deformation on the surface than the laser shock peening treatment, the compressive residual stress resulting from the SP is greater than the compressive residual stress resulting from laser shock peening (Ref 16). Xiao and co-authors (Ref 17) studied the effects of combining SP and plasma nitriding surface treatments. The authors understood that the defects generated by SP, used as a pre-treatment, enabled the formation of the nitrided layer and the nitrogen diffusion zone at lower temperatures. According to the authors, the SP pretreatment increased the level of surface energy and chemical reactivity, in addition to promoting a greater number of nitride nucleation sites on the surface. Finally, the authors reported grain refinement, promoted by the SP treatment; and increased resistance to delamination, promoted by the treatments combination (Ref 17). Tang et al. (Ref 5) studied the influence of the plasma molybdenizing and shot peening combination on the fretting fatigue and fretting wear resistances. According to the authors, the combination improved these properties by 27 times, calculating the volume loss of the alloy without treatment, treated only by SP, and treated by their combination. This result was attributed to compressive residual stress, higher surface hardness, and higher bonding between plasma-molybdenizied and titanium alloy. This bond, facilitated by the SP post-treatment, was promoted mainly by solid solution, and showed a distribution gradient from the surface, with differences in composition and hardness. SP treatment also increases surface roughness, which can induce stress concentration sites, thereby accelerating fatigue crack nucleation (Ref 18). Thus, the literature shows us that a combination of SP treatment with a surface chemical treatment can improve surface conditions while improving the mechanical performance of the titanium alloy.

Both SP and PIII treatments influence the residual stress field on the surface layers of a component. Compressive stresses on the surface hinder crack nucleation under both static and cyclic loads, contributing to improve the fatigue strength. The mechanisms responsible for the increase of fatigue life through the induction of compressive stresses can be (1) the increase of the period required for the crack to nucleate from the surface; (2) the increase of the crack propagation period by the reduction of the mean stress on the surface layers, and (3) the cases that the compressive stress moves the crack nucleation site to subsurface layers by protecting the surface (Ref 19).

The temperature of PIII surface treatment is another important variable to understand the tensile–tensile fatigue behavior. Increasing temperature during surface treatments increases coating thickness and, therefore, hardness, enhancing corrosion and wear resistances (Ref 20, 21). Regarding the fatigue strength of titanium alloys, an increase in temperature decreases ductility and contributes to pre-crack formation (Ref 20-22). Morita et al. (Ref 23) studied the effects of combined treatments (plasma nitriding, double heat treatment, and fine particle bombardment) on the wear and fatigue resistances of the Ti-6Al-4V alloy. The combined treatments improved the wear resistance, ultimate tensile strength (30%), and fatigue strength (59%) of the Ti-6Al-4V alloy (Ref 23). Hosseini and Ahmadi (Ref 20) studied the influence of plasma nitriding temperature on Ti-6Al-4V alloy wear resistance. According to their experimental results, changing the temperature from 700 to 850 °C increases the layer thickness, surface roughness, hardness, and wear resistance of Ti-6Al-4V alloy (Ref 21, 22). Farokhzadeh and Edrisy (Ref 24) studied nitride-coated Ti-6Al-4V alloy samples treated at 600 and 900 °C. The results demonstrated that an increase in temperature produces a thick nitride layer accompanied by an α-stabilized region, increasing fatigue life by at least two orders of magnitude (Ref 24).

The literature presents the effects of PIII treatment on the mechanical properties of metallic alloy surfaces. Studies showed, through ball-on-disk and potentiodynamic polarization tests, that PIII improves wear and corrosion resistances by up to an order of magnitude (Ref 25-29). Regarding tensile–tensile fatigue behavior, previous studies (Ref 30, 31) showed that the fatigue strength of Ti-6Al-4V alloy is maintained after PIII, especially in the low-cycle region. Compared to other surface treatments, such as physical vapor deposition or high-velocity oxygen fuel techniques, its deleterious effect is weaker in the low- and high-cycle fatigue regimes, even though PIII may introduce tensile residual stresses into surfaces. A combination of SP with other surface treatments maintains fatigue strength and improves wear resistance and the interfacial adhesion between the substrate and the coating (Ref 32, 33).

For over 20 years, the research group ‘‘Fatigue and Aeronautical Materials’’ has been studying the relation of applying surface treatments on metallic alloys and fatigue behavior. These analyzes were published for different deposition techniques and for different metallic alloys of aeronautical application (Ref 6, 12, 34, 35). When analyzing a material for aeronautical application, full knowledge of its performance, properties, and mechanical behavior diversity in the face of different solicitation conditions is necessary due to safety and costs, both material and immaterial, which are presented in a failure situation. This paper aims increasing the knowledge about Ti-6Al-4V alloy tensile–tensile fatigue behavior. And, not only that, but to present the PIII treatment as an alternative, that has already been proven to increase wear and corrosion resistances. Therefore, it is meaningful to evaluate the influence of PIII treatment on the fatigue resistance. Considering the relevance of shot peening treatment in the performance of metal alloys subjected to cyclic loading, we understand that the combination of treatments can not only guarantee the maintenance of the mechanical properties of the Ti-6Al-4V alloy, but also improve them. To the best of our knowledge, there have been no studies on the combined effects of PIII and SP on the tensile–tensile fatigue behavior of titanium alloys. The research gap of the present work was to analyze the influence of combined PIII treatment and SP (as a pretreatment) on the axial fatigue strength of the Ti-6Al-4V alloy.

2. Materials and Methods

2.1 Materials

The material used in this study was the Ti-6Al-4V alloy (5.8 Al, 0.03 C, 0.1 Fe, 0.002 H, 0.003 N, 0.106 O, 4.03 wt.% V, balance of Ti), received in the form of 12-mm-thick rods. The rods were supplied as wrought annealed Ti-6Al-4V ELI and presented specifications according to ASTM F-136 (Ref 36) (refer to the standard for mechanical, metallurgical, and mechanical specifications). The yield strength and tensile strength values obtained through tensile tests were 1000 and 1034 MPa, respectively. The microstructure exhibited an equiaxed annealed morphology with α phase (hexagonal) and β phase (body-centered cubic) in proportions of 76 and 24%, respectively. The average microhardness value was 336 $\pm$ 5 HV. Figure 1 presents the cross-sectional microstructure of the Ti-6Al-4V alloy with equiaxed microstructure.

2.2 Methods

2.2.1 Surface Treatments. The plasma immersion ion implantation (PIII) and shot peening (SP) surface treatments were performed both separately and combined on the fatigue specimens presented in Fig. 2. Measurements are in mm, and the region painted in green is the application area of the surface treatments.

The SP parameters were Almen intensity ranged between 0.41 and 0.49 mmA, 100% coverage, and media type of blasting S230 steel balls ($\varnothing$ = 0.7 mm) with a hardness value of 57 HRc. The process was carried out according to the AMS 2430 standard (Ref 37) and with other works reported in the literature that treated the Ti-6Al-4V alloy by shot peening for aeronautical application (Ref 38-40).

The PIII treatment was performed with 400 Hz and 7.0 kV parameters for 2 h with a pulse duration of 30 μs at two different temperatures: 500 °C (PIII 500) and 800 °C (PIII 800). A thermionic oxide cathode was used to produce electrons for bombarding the specimens. It also acted as an auxiliary heating system and increased the temperature to promote nitrogen diffusion. This technique was presented and described in a paper by Oliveira et al. (Ref 41).

2.2.1.1 Temperature Control. Temperature control during PIII treatment was necessary based on the design of the fatigue specimens. Figure 2 shows a diameter narrowing in the central region of the specimen, which induces stronger electronic bombardment in this region, thus the temperature exceeded the limit stipulated by the assay and modifying the microstructure of the sample. Initially, the treatment temperature increased to over 800 °C based on the combined effects of the auxiliary heating system and ion bombardment, promoting allotropic transformation and atomic diffusion. Therefore, the first performed treatment locally overcame 800 °C ($T_{\beta trans\text{-}sus} > 882$ °C) and resulted in the formation of a nitride layer on the surface and modification of the sample microstructure to a morphology known as Widmanstätten or lamellae. Figure 3 presents the microstructure of the material and the surface region of the PIII-nitrided sample at 800 °C (locally overheated) (Ref 31), which confirms the phenomenon described above.

Subsequent treatments were performed with temperature control in the central region of the specimen to ensure that the implantation would occur at the predefined temperature (i.e., 800 or 500 ° C). Figure 4 presents the microstructure of the material and the surface region of the SP + PIII-nitrided sample at 800 °C, where it can be observed the microstructure maintenance after the treatment.

2.2.2 Microstructural Characterization. *2.2.2.1 Microscopy Analysis.* Optical profilometry was performed using a Leica DCM3D device for surface roughness (Ra) measurement in an area of 1.27 $\times$ 0.95 mm^2 with 10 times magnification. Microhardness testing was conducted along specimen cross-sections using a Shimadzu HMV-2 T device. Fatigue fracture surfaces were analyzed via scanning electron microscopy (SEM) using a Leo 1450-VP device. Dislocation structures were investigated via transmission electron microscopy (TEM) using a TECNAI G2F20 device.

2.2.2.2 Residual Stress Analysis. Residual stress analysis was measured by the $\sin^2\psi$ x-ray method, under a Cu kα radiation source. The operation conditions were 40 kV and 30 mA with a counting time of 50.0 s and step size of 0.100°. Elastic modulus was kept constant, E = 113.4 GPa, and Poisson ratio of 0.321 (Ref 42, 43). This method provides a

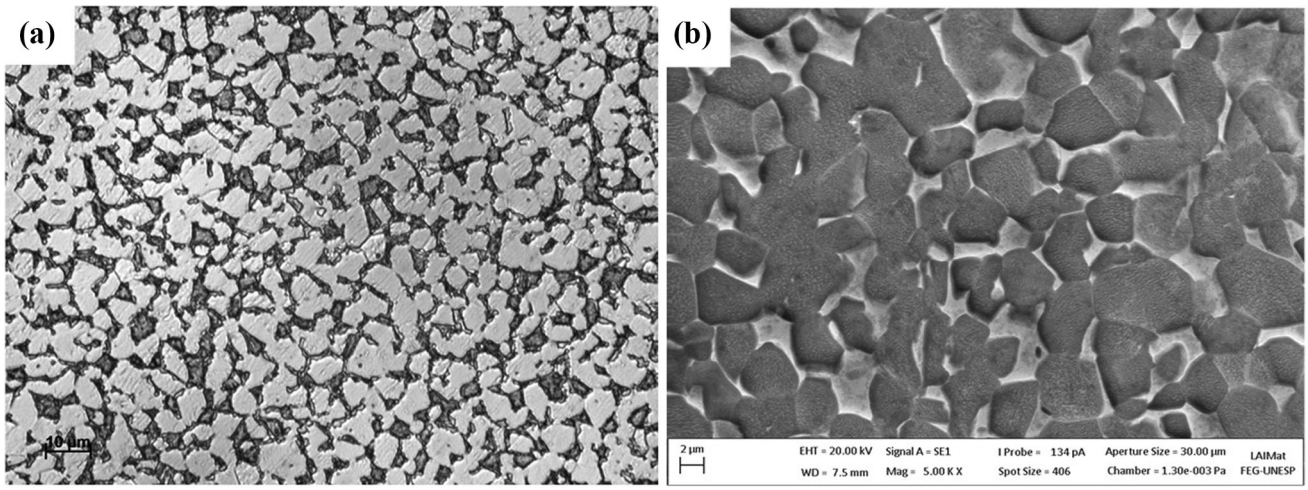

Fig. 1 (a) Optical microscopy (mag. = 500x) and (b) scanning electron microscopy (SEM) (mag. = 5000x) images of the as-received Ti-6Al-4V alloy

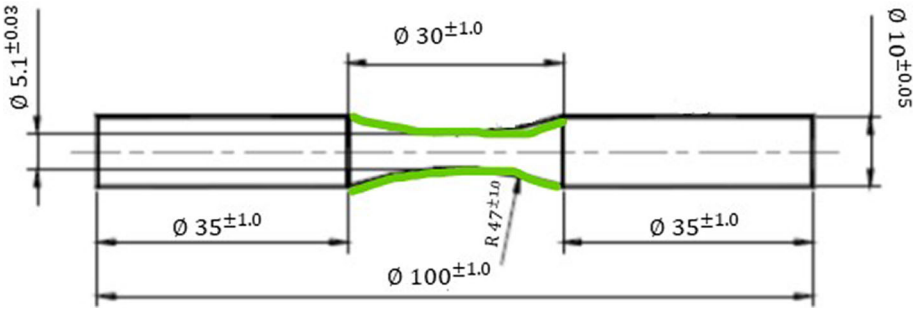

Fig. 2 Axial fatigue specimens

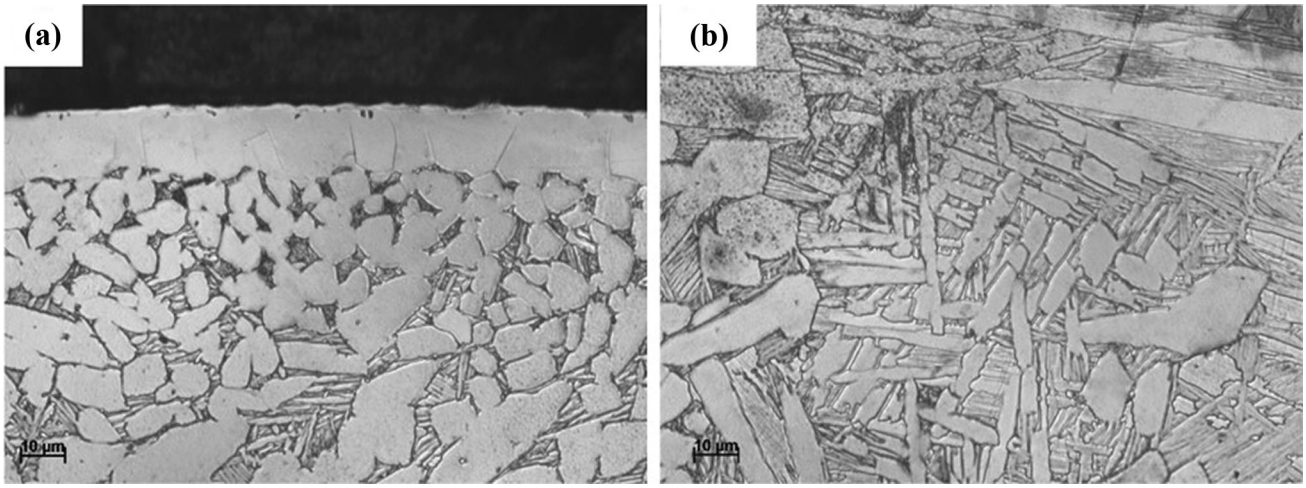

Fig. 3 Optical microscopy images of PIII-treated Ti-6Al-4V alloy at 800 °C: (a) nitrided layer + nitrogen diffusion zone and (b) lamellae morphology in the central region. Reproduced from Ref 32 under the terms of the Creative Commons Attribution License 4.0

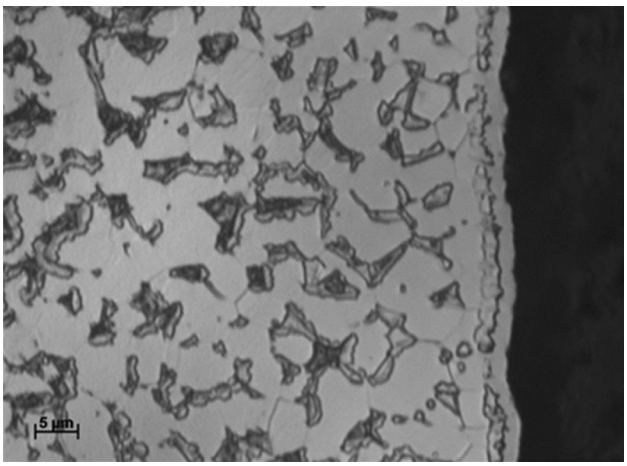

Fig. 4 Optical microscopy images of SP + PIII-treated Ti-6Al-4V alloy at 800 °C: nitrided layer + nitrogen diffusion zone and annealed morphology

measurement sensitivity of ± 20 MPa. The residual stress measurements were performed on specimens machined for fatigue testing in the center of the specimen, that is, in the center of the useful region that was subjected to surface treatments (green painted area of Fig. 2), in the longitudinal direction, for all experimental conditions.

2.2.3 Tensile–Tensile *Fatigue Tests*. Axial fatigue tests were conducted for all experimental conditions using an Instron 8801 device with a stress ratio (R) = 0.1 and frequency (f) = 10 Hz up to 10^6 cycles, or until fracture, at room temperature. The specimens were prepared according to the ASTM E466 standard (Ref 44) with a total length of 100 mm and minimum diameter of 5 mm. The S-N curves were analyzed to compare microstructures, the influence of SP, and treatment temperature effects. The fatigue samples tested conditions were the following:

a) Ti-6Al-4V: specimens in as-received condition, 15 essay.
b) SP: shot peened specimens, 9 essay.
c) PIII 800: Ti-6Al-4V alloy specimens treated with PIII at 800 °C without temperature control, 8 essay.
d) PIII 500: Ti-6Al-4V alloy specimens treated with PIII at 500 °C with temperature control, 11 essay.
e) SP + PIII 800: Ti-6Al-4V alloy specimens treated with PIII at 800 °C with temperature control and combined with SP as a pretreatment, 10 essay.
f) SP + PIII 500: Ti-6Al-4V alloy specimens treated with PIII at 500 °C with temperature control and combined with SP as a pretreatment, 5 essay.

2.2.3.1 Statistical Analysis. Weibull analysis was carried out and reported before (Ref 30), where the reliability and scatter of the results were analyzed. According to the ISO 12107 standard (Ref 45), tests with a small number of samples

can be used for exploratory studies. The number of samples used here gives us a 50% probability of failure with 95% reliability for tests with five samples; and a probability of failure of 10% with a reliability of 50% for tests with nine samples.

A statistical analysis of the fatigue data based on ASTM E739 (Ref 46) was performed for all experimental conditions using stress-life (S-N) linear regression models. The analysis includes normality tests, regression plots, prediction intervals, confidence bands for a confidence level of 95%, and residual plots. The statistical analysis aimed to assure the reliability of the fatigue data and the findings in this paper.

3. Results

3.1 Ti-6Al-4V Tensile–Tensile Fatigue Behavior

The tensile–tensile fatigue behavior was investigated for the conditions: (1) base material (Ti-6Al-4V), (2) shot peened Ti-6Al-4V alloy, (3) PIII treated at 800 °C (PIII 800), (4) PIII treated at 500 °C (PIII 500), (5) PIII treated at 800 °C after SP pretreatment (SP + PIII 800), and (6) PIII treated at 500 °C after SP pretreatment (SP + PIII 500). Figure 5 presents the S-N curves for the tests performed with amplitude stress levels in the range between 100 and 450 MPa.

As mentioned previously, the PIII 800 treatment without temperature control changed the microstructure from equiaxed to a lamellar morphology. The morphology changed because the treatment overcame the allotropic transformation temperature, β transus ($T > 882$ °C) (Ref 30, 31). This treatment also produced a layer composed of a nitrogen diffusion zone and nitrides ((N (α) + Ti_2N + TiN) with a total thickness of 13.4 μm (Ref 31).

Table 1 lists the theoretical equations obtained from the experimental axial fatigue data, and the calculated fatigue strength values for all experimental conditions. The equations and calculated lifetimes (N) were obtained from the fatigue tests, shown in Fig. 5, using minimum squares method. Despite increasing surface roughness, the SP process preserves the Ti-6Al-4V alloy's axial fatigue strength in the low-cycle fatigue regime ($N = 10^4$). For high-cycle fatigue (low-stress levels), surface roughness plays an important role and SP treatment decreases the fatigue strength of the Ti-6Al-4V alloy.

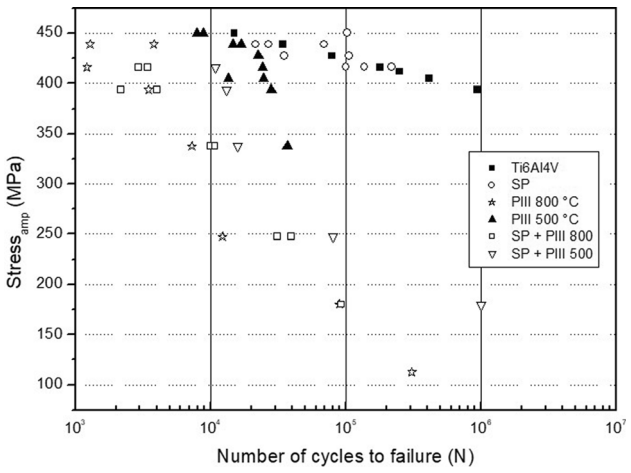

Fig. 5 Ti-6Al-4V alloy S-N curves: untreated (Ref 10), SP, PIII 800 (Ref 11), SP + PIII 800, PIII 500, and SP + PIII 500 treatment conditions

Figure 6 shows an S-N relationship, according to the model log σ *versus* log N.

The experimental results of this study allow an interpretation of Fig. 6, relating the effects of microstructure and temperature on tensile–tensile fatigue behavior: the slopes of the curves show the influence of microstructure and temperature on tensile–tensile fatigue behavior. It is interesting to note that, for the untreated and SP conditions, which were not subjected to a heat treatment, there was the typical slope that represents the annealed microstructure. It is noted that the surface treatment increased the fatigue strength proportionally. And, once one knows the microstructure and its behavior, we can predict the fatigue strength for both, high and low cycle regimes. However, for the PIII 500 and SP + PIII 500 conditions, the slope was modified for the same microstructure (untreated, SP, PIII 500 and SP + PIII500 have the same core microstructure). Here, it can be said that the action of temperature changed the slope, due to promoting atomic diffusion and non-conservative dislocation slipping (Ref 7). Thus, the action of temperature changed the slope of the curve, but the proportionality between the conditions PIII 500 and SP + PIII 500 is still observed, since the microstructure was maintained. Therefore, for project purposes, surface treatments that involve temperature application, capable of activating diffusion mechanisms, even with the morphology maintenance, exert an influence on tensile–tensile fatigue behavior. Finally, the slopes of the curves in the PIII 800 and SP + PIII 800 conditions were different due to the microstructural difference: in the PIII 800 condition, there was lamellar microstructure, in the SP + PIII 800 condition, there was equiaxed microstructure.

The surface residual stress values for the Ti-6Al-4V alloy under untreated, SP, PIII 500, SP + PIII 800, and SP + PIII 500 conditions are listed in Table 2. The residual stress was calculated with varying ψ angles at four different inclinations. The strong diffraction can be founded at $\psi = 0°$ in the HC titanium planes {103} and {213}, and were detected with a diffraction angle (2 θ) of 70.6° and 139.4º, respectively (Ref 45, 47, 48).

3.2 Fractures Aspects and Deformation Mechanisms

Figure 7, 8, 9, 10, 11, and 12 presents the main fracture aspects for all experimental conditions considered in this study in the low-cycle fatigue region, where the Ti-6Al-4V alloy's fatigue life increased or remained the same.

Figure 7, 8, and 9 shows the typical fatigue fractures with nucleation plus propagation and well-defined final fracture zones. The details (Fig. 7b, c and 8b) show that the fracture started at a single point on the surface and propagated radially toward the center. The plane strain fracture zone was characterized by plastic deformation and dimples. Figure 9b shows a continuous white coating (red arrow) on the surface and the single nucleation point (white arrow), where there was a gap on the coating.

Figure 10 shows a fracture with more than one superficial nucleation point. In this treatment condition, where the surface has both the nitrided layer and the shot peening modification, the local mean stress is not high enough to make the crack grow from the surface. As the sample is being subjected to cyclic deformation in a low-cycle regime, to maintain its integrity for

Table 1 Calculated fatigue strength for 10^4, 10^5, and 10^6 cycles

			Number of cycles, N		
			10^4	10^5	10^6
Calculated fatigue strength, MPa	Ti-6Al-4V	$\log N = 18.6 - 0.014\sigma$	1043	971	900
	Shot peened Ti-6Al-4V	$\log N = 11.1 - 0.00652\sigma$	1089	936	782
	PIII 800	$\log N = 6.1 - 0.00295\sigma$	712	373	34
	PIII 500	$\log N = 6.35 - 0.00227\sigma$	1035	595	154
	PIII 500 + SP	$\log N = 7.14 - 0.00355\sigma$	884	603	321
	PIII 800 + SP	$\log N = 7.03 - 0.00436\sigma$	695	466	236

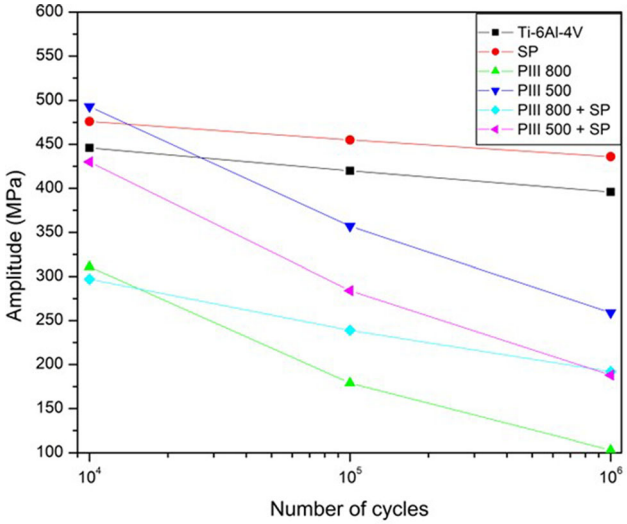

Fig. 6 Ti-6Al-4V alloy S-N curves according to the model log σ versus log N: untreated, SP, PIII 800, SP + PIII 800, PIII 500, and SP + PIII 500 treatment conditions

Table 2 Ti-6Al-4V alloy residual stress under untreated, SP, PIII 500, PIII 800 + SP, and PIII 500 + SP conditions

	Diffraction plane	Residual stress, MPa
Ti-6Al-4V	{103}	− 127 ± 28
Shot peened Ti-6Al-4V	{103}	− 119 ± 68
PIII 500	{103}	189 ± 51
PIII 500 + SP	{213}	23 ± 10
PIII 800 + SP	{213}	187 ± 30

a longer time, the small cracks nucleate at various points on the surface so that they can overcome the compressive stress and propagate to the center of the sample.

Figure 11 presents cleavage surfaces (Fig. 11a and b), multiple crack nucleation sites on the surface (dotted region in Fig. 11a), and heterogeneous deformation (Fig. 11c). In the SP + PIII 800 condition, Figure 12, the α shell and the nitride coating make the surface brittle (Fig. 12b). This brittleness offers no resistance to crack growth in the initial stages of crack propagation when the growth rate should be relatively low. Multiple crack nucleation sites (dotted region in Fig. 12a), a tensile fracture morphology (Fig. 12a), and heterogeneous deformation (Fig. 12c) can be observed for this condition.

Figure 13 presents the dislocation structures of the Ti-6Al-4V alloy in the untreated condition after a fatigue process conducted at 950 MPa.

Table 3 shows the properties of the tensile tests for Ti-6Al-4V alloy, with yield stress (σ_{ys}), ultimate tensile strength (σ_{UTS}).

Empirical equations Eq 1, such as Hollomon's model, may be used to represent the true stress (σ_T) and true strain (ε_T) relationship. The k (1466 MPa) parameter is the strength coefficient, whereas the n-exponent (0.097) is related to the strain-hardening ability of metallic materials.

$$\sigma_T = k\varepsilon_T^n \quad \text{(Eq 1)}$$

The effect of cyclic loading on the Ti-6Al-4V alloy can be enriched based on the analysis of tensile properties and parameters from Hollomon's equation Eq 1 (Ref 49). The analyses, proposed by Manson and Hirschberg (Ref 50), use monotonic properties to define whether a material will soften or harden under cyclical conditions. Based on Table 3, the σ_{UTS}/σ_{YS} ratio of 1.06 and the strain-hardening exponent, $n = 0.097$, have been determined in the present study. The σ_{UTS}/σ_{YS} ratio and n-exponent can define the ability of a material to undergo cyclic softening or hardening, as reported by Manson and Hirschberg (Ref 50). In this context, if $\sigma_{UTS}/\sigma_{YS} < 1.2$, the material tends to soften. When $\sigma_{UTS}/\sigma_{YS} > 1.4$, the material hardens. For ratios between the limits presented, the forecast is difficult, although significant changes in cyclic properties are not expected. The strain-hardening exponent plays an important role in predicting cyclic softening and hardening of engineering alloys. If $n > 0.20$ or $n < 0.10$, the material is likely to harden or softening, respectively. Thus, based on values in the present work, there is evidence Ti-6Al-4V alloy undergoes cyclic softening.

3.3 Statistical Analyses

The fatigue data were statistically analyzed based on the standard practice for statistical analysis of linear stress-life (S-N) regression models. The present analysis was important to assure the reliability of the fatigue data. Furthermore, the statistical regression analysis relies on population normality, and, therefore, it was important to apply a normality test to determine the normality of the fatigue data before the regression analysis.

Figure 14 shows the normality probability test of the fatigue data for all experimental conditions. The methodology was based on the Ryan-Joiner statistics with a confidence level of 95% ($\alpha = 0.05$). The correlation coefficient for Ti-6Al-4V base material, SP, PIII 800 °C, PIII 500 °C, SP + PIII 800 °C, and SP + PIII 500 °C conditions were 0.949, 0.969, 0.952, 0.985,

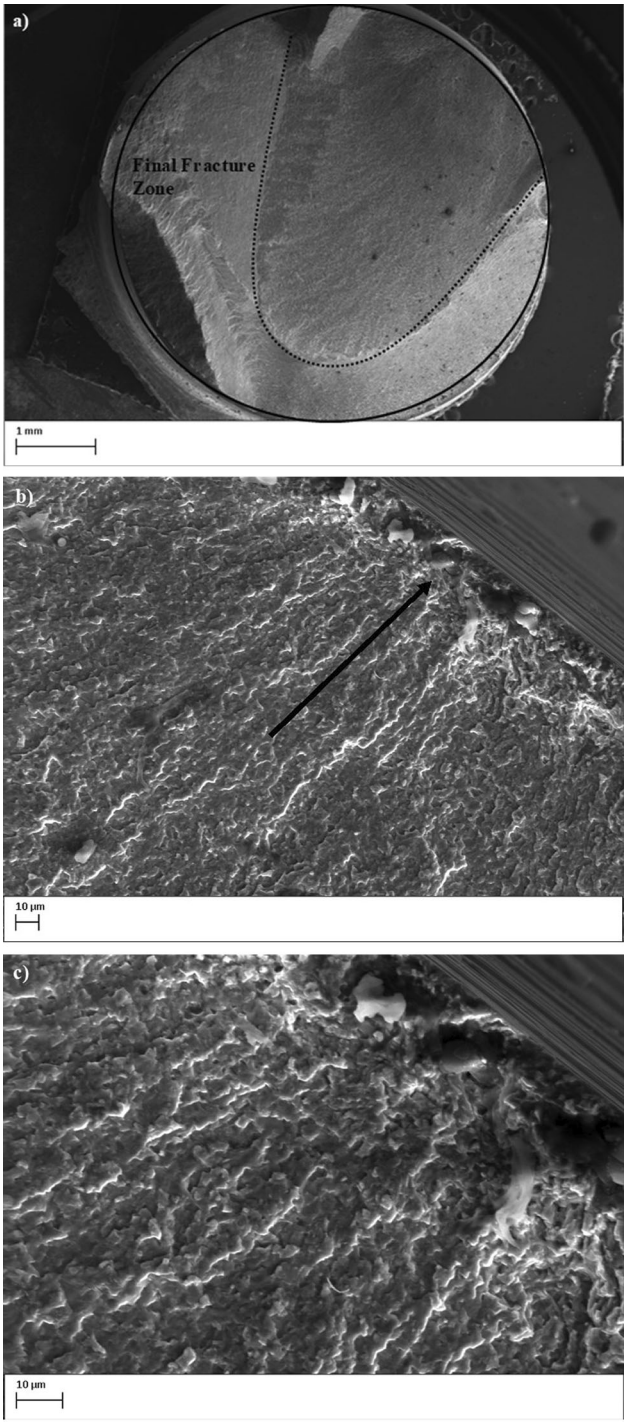

Fig. 7 Ti-6Al-4V alloy fatigue fracture in the untreated condition, 975 MPa: (a) fracture overview (mag. = 35X), (b) fracture origin (nucleation site, mag. = 1000X), (c) fracture origin (nucleation site, mag. = 2000X)

0.967, and 0.902, respectively. The Ryan-Joiner statistic assessed the strength of the correlation between the fatigue data and the normal scores of the data. It can be observed that even the smaller coefficient, obtained for the SP + PIII 500 °C condition, was higher than 0.900. Since the correlation coefficient was close to 1 for all experimental conditions, the logarithms of the fatigue lives can be considered normally distributed.

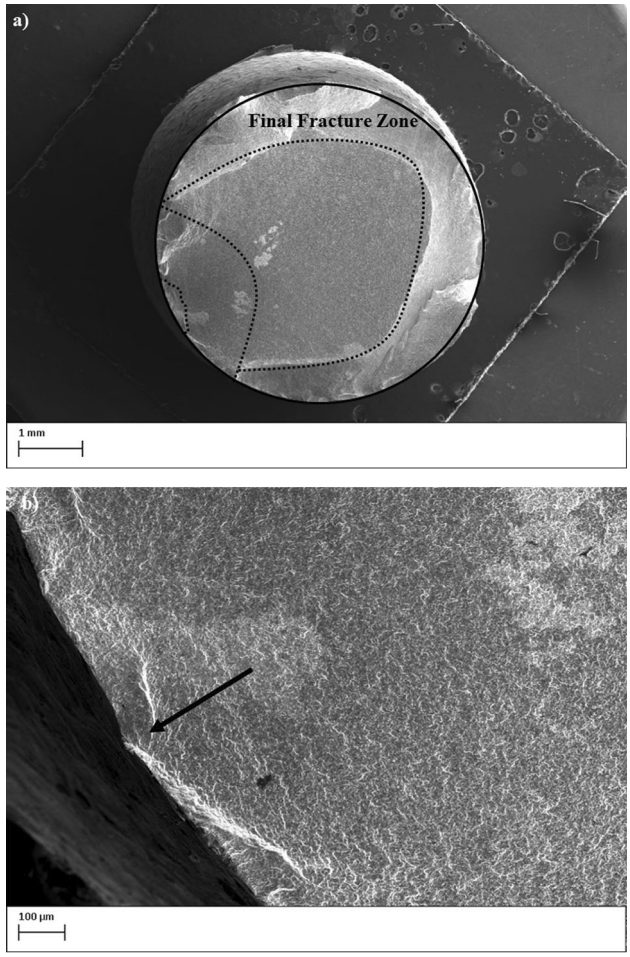

Fig. 8 Ti-6Al-4V alloy fatigue fracture in the SP condition, 975 MPa: (a) fracture overview (mag. = 28X), (b) fracture origin (nucleation site, mag. = 200X)

Further methods used to assess the normality of the fatigue data were the P-value analysis and the graphical technique. The P-value analysis confirmed the fatigue data's normality for SP, PIII 800 °C, PIII 500 °C, SP + PIII 800 °C, and SP + PIII 500 °C since the *P*-values were higher than the significance level of 0.05 (confidence level of 95%). For the Ti-6Al-4V base material, the normality was also confirmed since the P-value was nearly similar to 0.05, and the number of experimental points was at least $N = 20$. The graphical technique could also successfully confirm the normality of the results since the plotted points in Fig. 14 were approximately straight lines. Finally, the experimental data normality assures the reliability of statistical analysis and regression models applied.

Linear regression models were applied to the fatigue data for all experimental conditions. Figure 15 shows that the linear regression models provided a fitted line plot with high or suitable adjustments to the experimental data with coefficients of determination R-sq for Ti-6Al-4V base material, PIII 800 °C, PIII 500 °C, SP + PIII 800 °C, and SP + PIII 500 °C of 77.6, 92.6, 64.9, 96.8, and 90.0%, respectively. The only condition that did not fit an appropriate value of the coefficient of determination was the SP, mainly due to some points as outliers of the 95% confidence bands. The R-sq is a statistical measure of the adjustment of the experimental data to the fitted regression model. Therefore, the linear regression

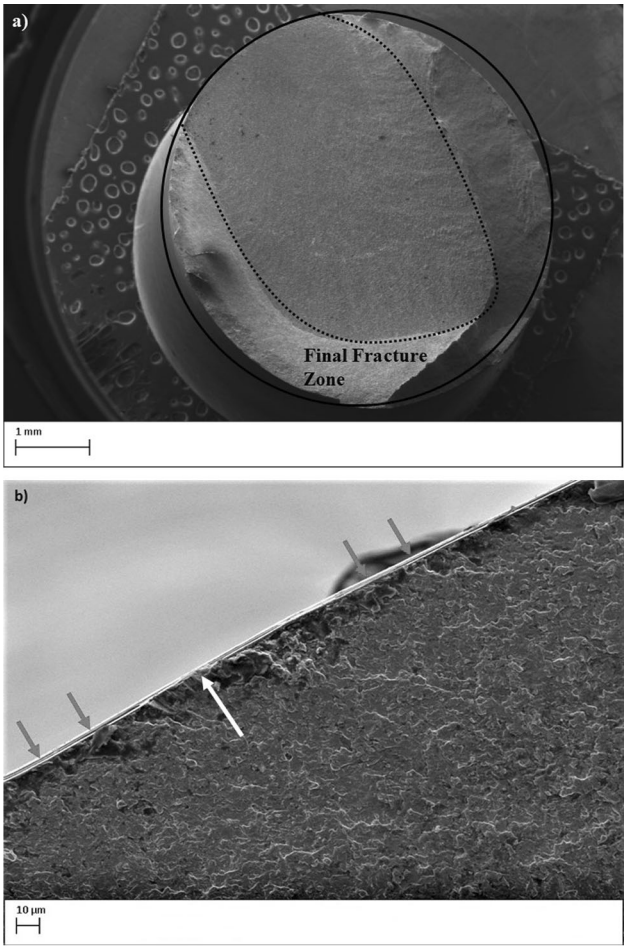

Fig. 9 Ti-6Al-4V alloy fatigue fracture in the PIII 500 condition, 875 MPa: (a) fracture overview (mag. = 34X), (b) fracture origin (nucleation site, mag. = 1000X)

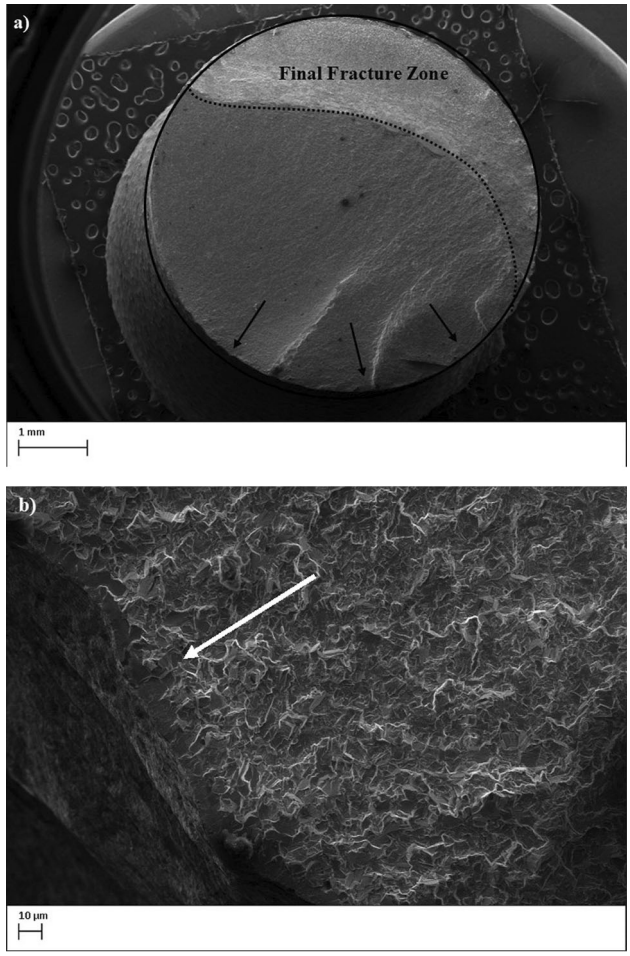

Fig. 10 Ti-6Al-4V alloy fatigue fracture in the SP + PIII 500 condition, 875 MPa: (a) fracture overview (mag. = 30X), (b) fracture origin (nucleation site, mag. = 1000X)

model explains, for example, 96.8 and 90.0% of the experimental data for the SP + PIII 800 °C and SP + PIII 500 °C conditions, respectively.

Figure 15 also presents the 95% confidence bands for the entire median S-N curve computed according to ASTM E739 (Ref 46). The confidence intervals (CI) are hyperbolic bands where the regression model equation is included in 95% of the cases. Considering the plotted confidence interval, it was possible to observe which points were within the 95% confidence range. While the CI consider the confidence for the mean of values, the prediction intervals (PI), also plotted in Fig. 15, allow the observation of points within the 95% prediction range of likely values for each single point response. As expected, the PI were always wider than the corresponding CI because predicting a single response value is less certain than predicting the mean response value. The only experimental point out of the 95% prediction interval occurred for the fatigue data of the Ti-6Al-4V base material, which has the higher number of specimens in the population.

The S-N curves of Fig. 15 show a high occurrence of points within the CI, supporting the statistical reliability of the linear regression models applied. It can be observed wider confidence bands for the SP and SP + PIII 500 °C conditions compared to the other conditions tested due to the variability of results and number of experiments, respectively. However, all the experimental points of the SP + PIII 500 °C condition were within the 95% confidence bands, which indicated the low variability and the reliability of the results despite the lower number of experiments performed in this condition. Moreover, for the SP + PIII 800 °C and Ti-6Al-4V base material conditions, the narrow confidence bands indicated the low variability of the fatigue data and the sufficiently large number of experiments.

The analysis of variance (ANOVA) of the linear regression models resulted in *P*-values of approximately 0.000 for PIII 800 °C, SP + PIII 800 °C, and Ti-6Al-4V base material. For PIII 500 °C, SP + PIII 500 °C, and SP, the *P*-values were 0.003, 0.014, and 0.151. Except for the SP, all conditions resulted in significantly lower *P*-values than the adopted significance level of 5% (0.05), proving the statistical significance of the linear regression models. As previously discussed, the outlier points for the SP condition were responsible for its inadequate adjustment to the linear regression model. The ANOVA also confirmed the high statistical significance of the fatigue data results through the high F-values obtained for the experimental conditions. For example, for the SP + PIII 800 °C condition, a high F-value of 209.88 was obtained in the ANOVA of the linear regression model.

The residual plots analysis was also performed to verify the fit of the regression models for all experimental conditions. The residuals are the difference between an observed value and its

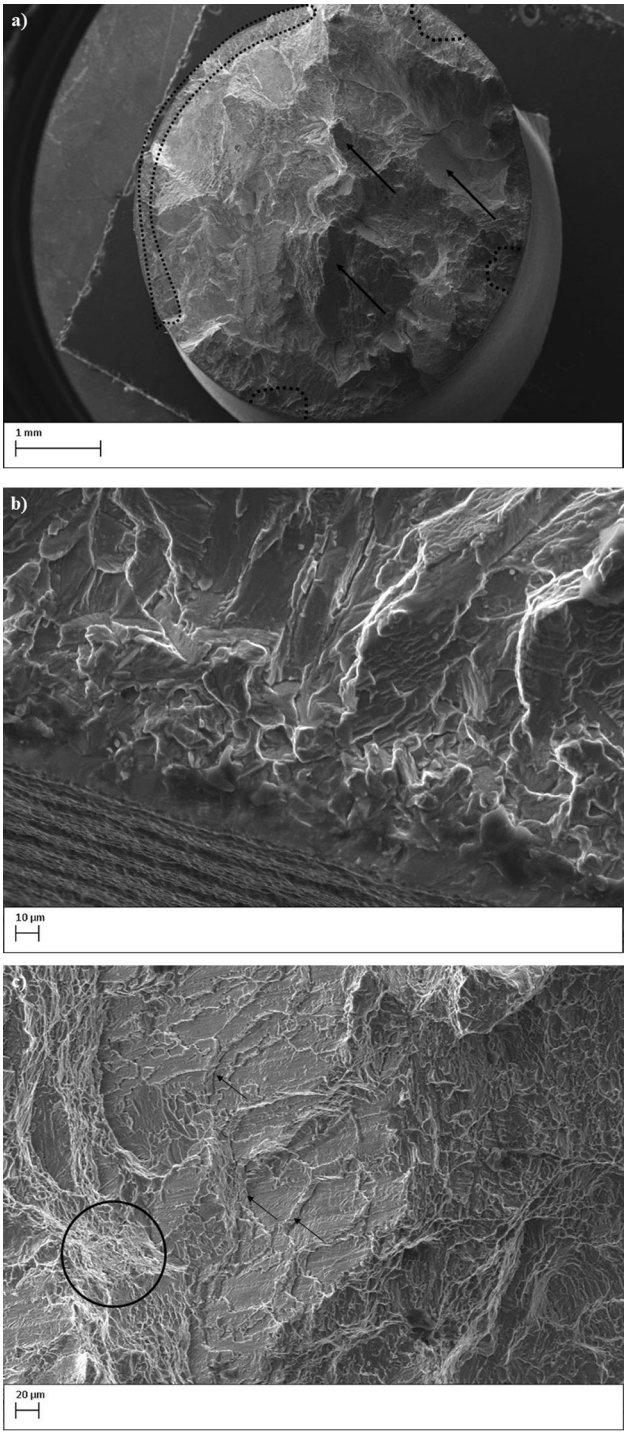

Fig. 11 Ti-6Al-4V alloy fatigue fracture in the PIII 800 condition, 975 MPa: (a) fracture overview (mag. = 37X), (b) nucleation site (mag. = 1000X), (c) final fracture zone (center, heterogeneous deformation, mag. = 500X)

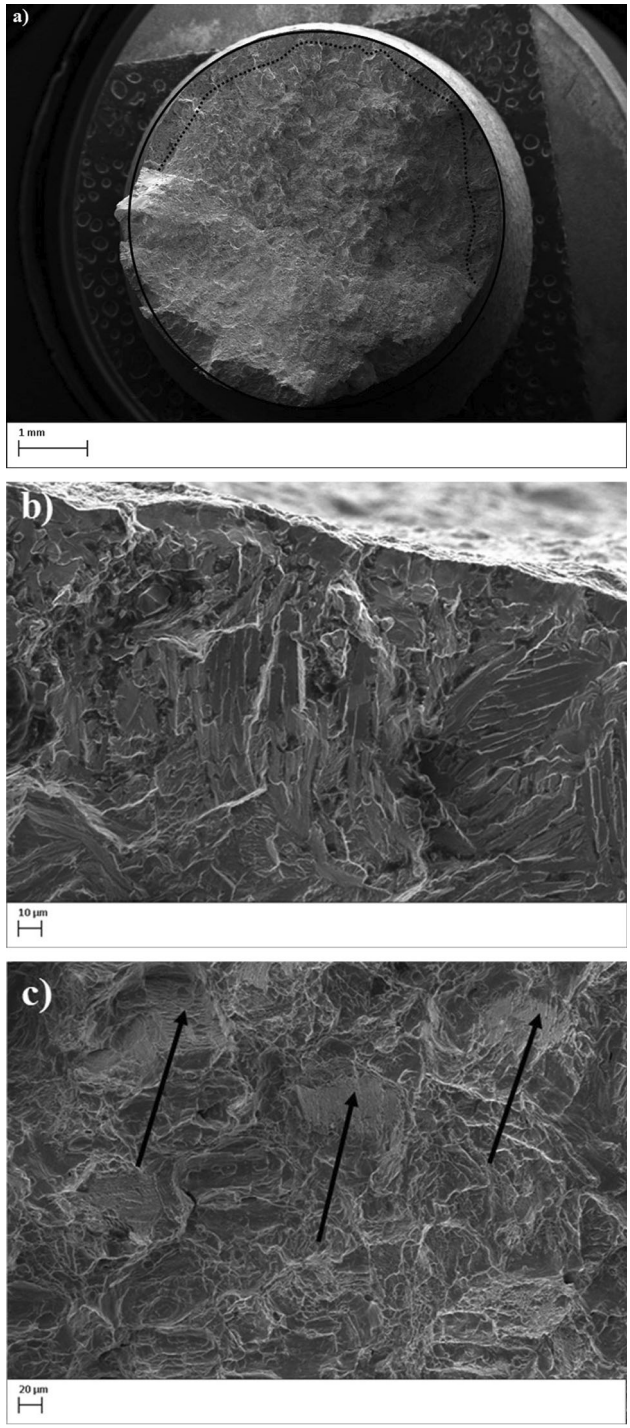

Fig. 12 Ti-6Al-4V alloy fatigue fracture in the SP + PIII 800 condition, 875 MPa: (a) fracture overview (mag. = 30X), (b) nucleation site (mag. = 1000X), (c) final fracture zone (heterogeneous deformation, mag. = 500X)

corresponding fitted value in the linear regression model. Figure 16 displays the residuals plots of the linear regression model for the PIII 800 °C condition as an example of the behavior of the residual plots observed in the fatigue data of this work. The obtained normal probability plots follow a straight line showing that the residuals are normally distributed and proving the non-existence of outliers or discontinuities. The residuals versus fits and residuals versus order plots indicated a similar tendency of dispersion of the residual data without any patterns associated. The histogram of residuals confirmed the symmetric tendency of results within the model with the highest frequency in the center of the histogram (residual of zero). Therefore, the linear model goodness-of-fit was confirmed by the residuals plots analysis.

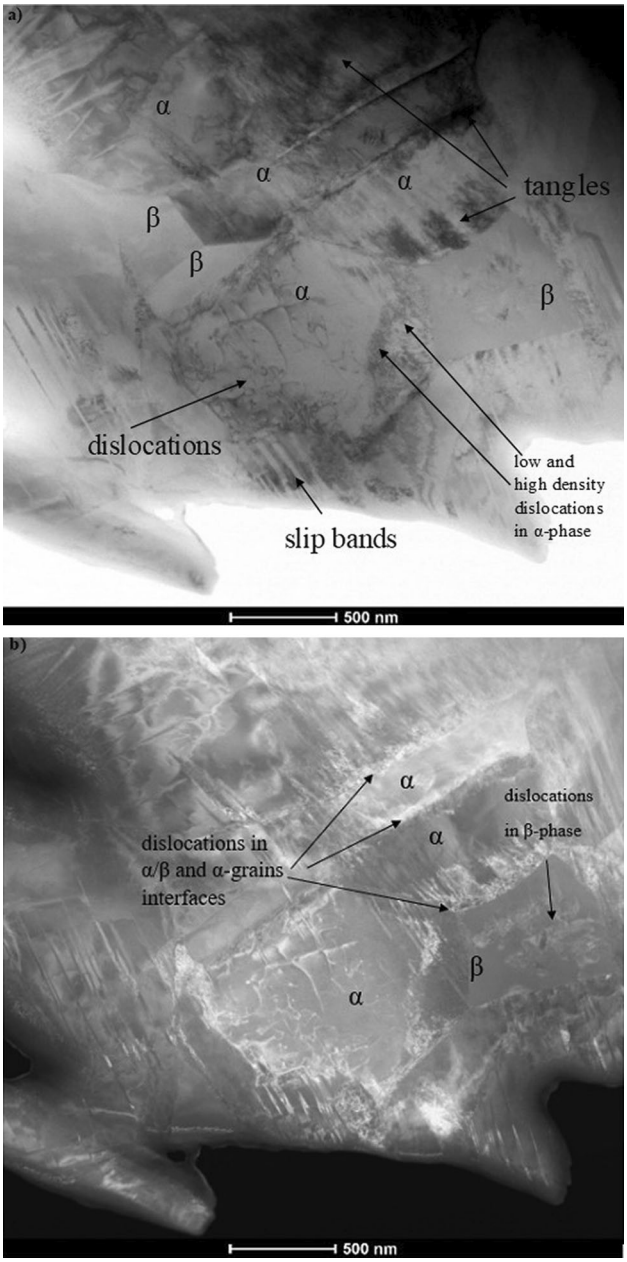

Fig. 13 TEM image of untreated Ti-6Al-4V alloy, fractured at 950 MPa with an annealed microstructure: a) bright-field TEM, (b) dark field-TEM

Table 3 Tensile properties of Ti-6Al-4V alloy

σ_{YS}, MPa	σ_{UTS}, MPa	*K*, Mpa	*n*
990 ± 6	1050 ± 9	1466 ± 4	0.097 ± 0.006

4. Discussion

This section will be devoted to further discussing the results by comparing them with each other and with the literature. The discussion will begin with the PIII 800 condition, which, due to its experimental conduction, resulted in a material with a lamellar morphology combined with a nitrided layer.

The fatigue behavior of a lamellar $\alpha + \beta$ titanium alloy depends on colonies, lamellae thickness, crystallographic orientation, and grain boundary geometry. Studies on crack propagation and damage tolerance in lamellar $\alpha + \beta$ titanium alloys have shown a decreased crack propagation rate, with energy loss based on crack deflection (Ref 51, 52). Crack propagation in a lamellar microstructure is retarded by the lamellae and colonies, which act as barriers to dislocation slipping (Ref 51-53).

Griza et al. (Ref 54) studied the influence of the Ti-6Al-4V alloy's microstructure on its mechanical properties. They determined that a fine globular microstructure was more resistant to fatigue than a lamellar structure. Further studies are required to identify the thermal treatment conditions that will form a lamellar microstructure to achieve a combination of crack propagation resistance, ductility, and fatigue resistance. Table 1 shows that the PIII treatment conducted at 800 °C (PIII 800) reduced the axial fatigue strength in both the low- and high-cycle fatigue regimes, with a stronger effect in the high-cycle regime. The fatigue strength reduction for the PIII 800 condition can be attributed to ductility loss, ceramic layer formation, and increasing α phase proportion in the Ti-6Al-4V alloy based on nitrogen diffusion (α phase stabilizer) (Ref 31). The fatigue behavior association with material ductility variation was reported by Soltani-Tehrani et al. (Ref 55). According to the authors, who conducted fatigue tests on Ti-6Al-4V alloy manufactured by laser powder bed fusion, the alloy fatigue resistance, made with a coarse powder, increased due to ductility, and decreasing of defects size (Ref 55).

In the PIII 500 condition, the Ti-6Al-4V alloy microstructure was maintained. The discussion will present, here, the importance of the nitrided layer as a surface protection and improvement component of tribological characteristics, which for titanium, represent its class of properties more critical (Ref 1, 7, 26).

The PIII 500-treated axial fatigue strength (1035 MPa) was close to that of the untreated Ti-6Al-4V alloy (1043 MPa) in the low-cycle fatigue regime (Table 1). This is a noteworthy result when considering that PIII improves the corrosion and wear resistances of the Ti-6Al-4V alloy (Ref 25-27) while maintaining the low-cycle fatigue strength. In the high-cycle fatigue regime (i.e., $N = 10^6$ cycles), the fatigue strength was significantly reduced (154 MPa).

Analyzing the SP treatment influence on the Ti-6Al-4V alloy, either alone or combined with the PIII treatment, three microstructural aspects must be taken into account: (1) the presence of compressive residual stresses on surface; (2) surface hardness; (3) the surface roughness; (4) nitrogen diffusion rate.

Compressive stresses on the surface and subsurface layers delay the crack nucleation and propagation periods since such stresses tend to reduce the mean stress on the surface layers and induce crack closure. Increased roughness contributes to the presence of stress concentration sites, thereby accelerating crack nucleation. The balance between the beneficial effects of the compressive residual stress field and the worsening of the surface finish defines the fatigue behavior of the SP condition. The SP effect causes distortion in the crystalline structure, increases the dislocation density, and improves the resistance to crack nucleation by work hardening, which varies according to the SP intensity (Ref 34, 56-58).

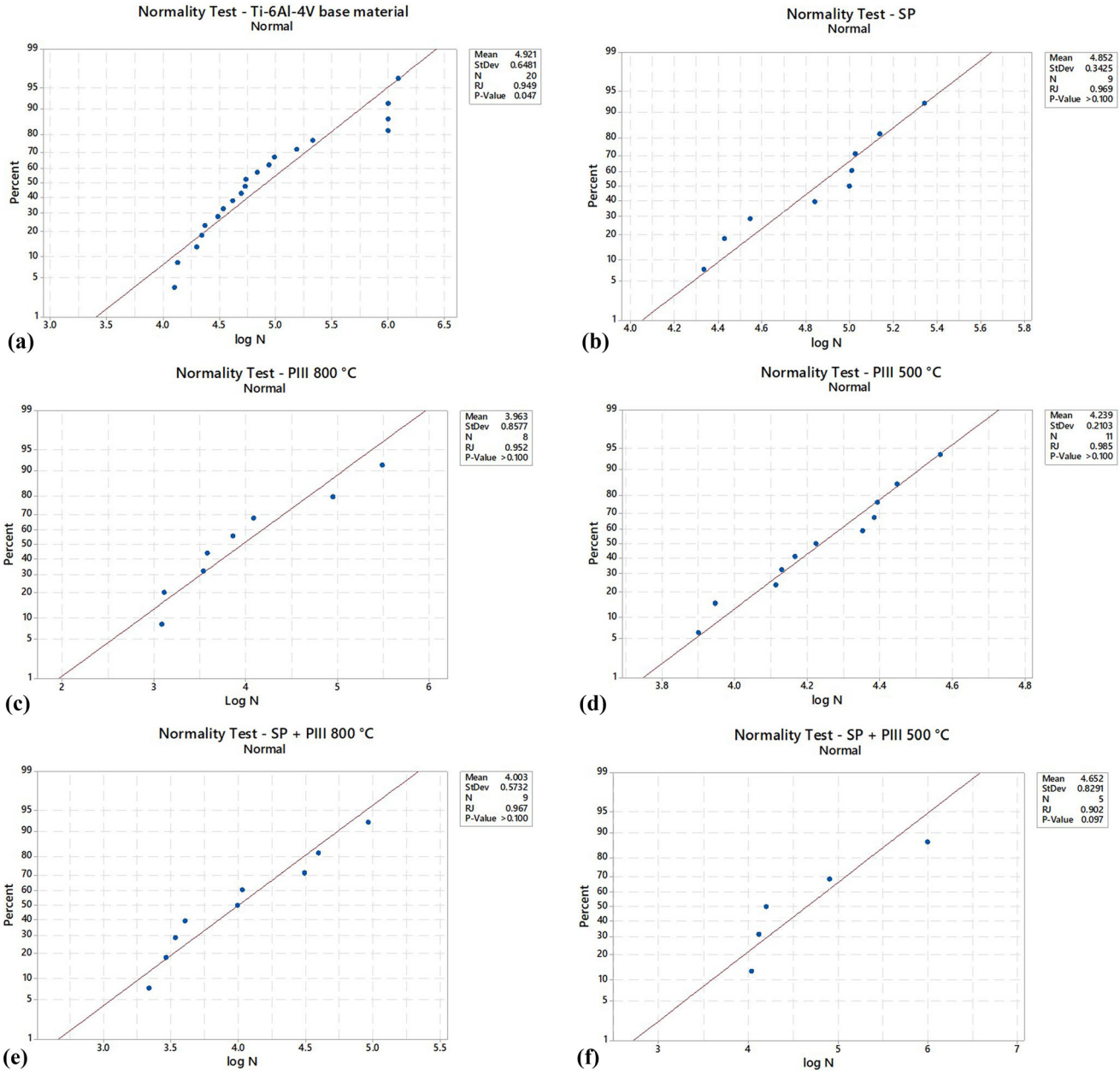

Fig. 14 Ryan-Joiner normality test of the (a) Ti-6Al-4V base material, (b) SP, (c) PIII 800 °C, (d) PIII 500 °C, (e) SP + PIII 800 °C, and (f) SP + PIII 500 °C

In this work, the mean surface roughness after the SP process was Ra = 5.88 ± 0.49 μm. A comparison between the Ra values of untreated (Ra = 1.00 ± 0.28 μm) (Ref 30) and SP treatment conditions revealed an increase in roughness of more than five times after the SP treatment. The surface microhardness values for untreated and SP conditions were equal to 336 ± 9 HV and 365 ± 10 HV, respectively. To summarize, the SP treatment induced compressive residual stress on the surface and increased the hardness. However, the surface roughness increased. Table 2 shows that the residual stress values were − 127 and − 119 MPa for the untreated and SP conditions, respectively. Both conditions exhibited compressive residual stresses near the surface, inducing a compressive residual stress field in the surface layers (Ref 33).

From Table 1 and Fig. 5, one can conclude that the SP process with the parameters used in this work has a negligible effect on the Ti-6Al-4V alloy's low-cycle axial fatigue strength ($N = 10^4$), because of the balance between the residual stress field and the surface roughness. The SP process, used as pre-treatment, increased the axial fatigue strength for lifetimes of 10^5 cycles (603 MPa) and 10^6 cycles (321 MPa) when compared to the PIII 500 condition (Table 1). Furthermore, the SP process was important for the tensile–tensile fatigue behavior when combined with PIII treatment. Considering the standard deviations, the shot peening treatment did not change the residual stress value of the untreated material, which already had a compressive character. Understanding this result requires further investigation. Here, it can be said that the chosen shot peening treatment condition benefited tensile–

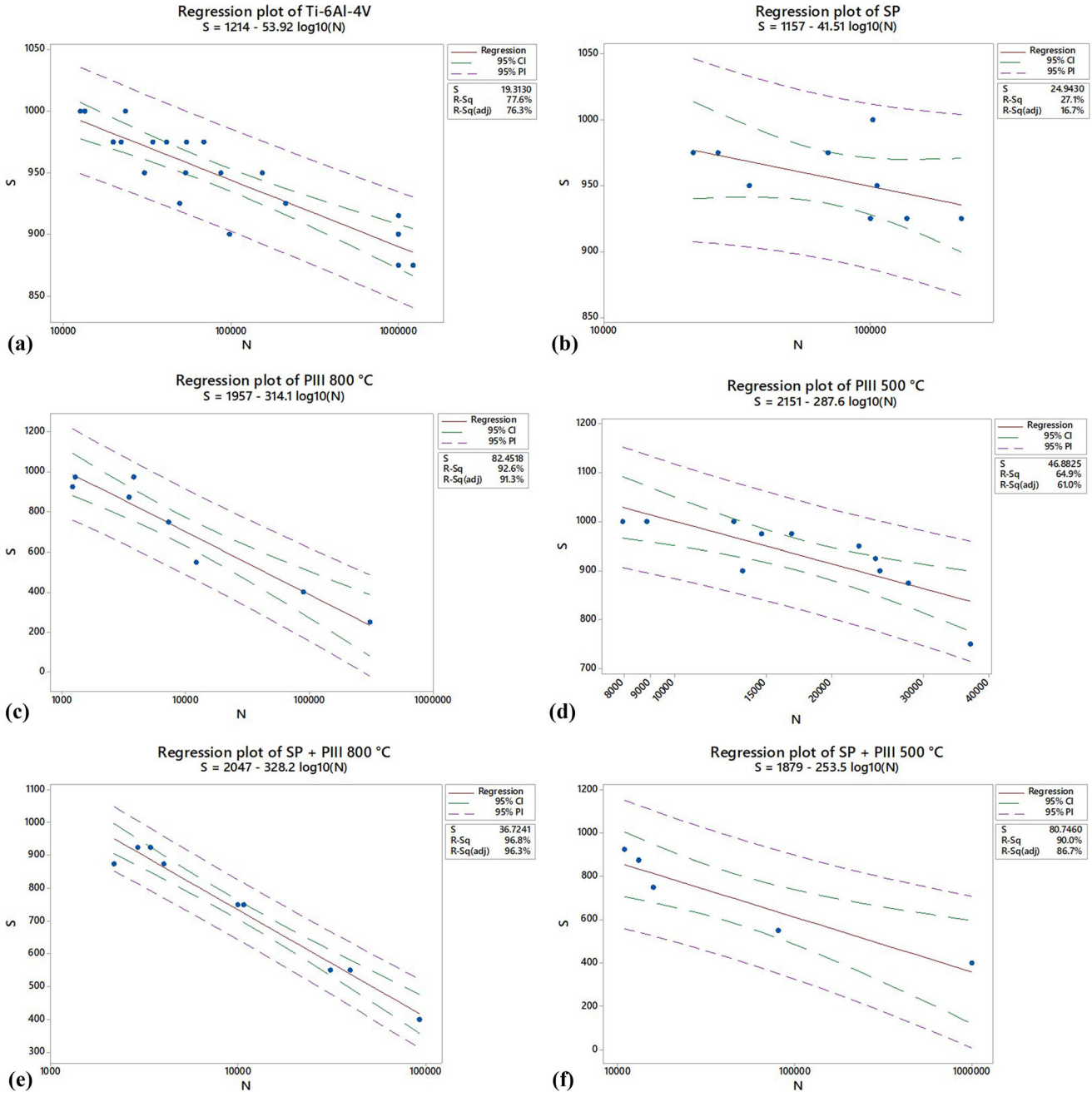

Fig. 15 Linear Regression plot of the (a) Ti-6Al-4V base material, (b) SP, (c) PIII 800 °C, (d) PIII 500 °C, (e) SP + PIII 800 °C, and (f) SP + PIII 500 °C

tensile fatigue performance and decreased the residual stress value on surface when associated with PIII treatment.

According to Kovaci et al. (Ref 58), the surface modifications generated by the SP treatment (dislocations density increase, new grains and subgrains formation) open new paths for nitrogen diffusion. In this case, the activation energy for nitrogen diffusion decreases, increasing its diffusion rate in the Ti-6Al-4V alloy. Thus, the combination of the SP with the PIII 800 treatments resulted in a constructive combination, regarding the formation of a nitrided layer, which depends on the diffusion of nitrogen in the titanium (Ref 58). This effect, when analyzed within the context of this work, which is fatigue performance, can be harmful. Yetim et al. (Ref 59) reported that the difference between the elastic modulus of the Ti-6Al-4V alloy and the nitrided layer (TiN + Ti2N) is almost four times. Thus, during cyclic deformation, the metallic core of the alloy undergoes a high level of elastic deformation, at a much higher level than its nitrided surface. This difference in stress concentration between the surface and the center of the sample results in the formation of cracks on the surface (Ref 59). These cracks, therefore, nucleated in a rigid ceramic layer, and propagate quickly to the metallic center of the sample, regardless of the hardness of the nitride layer. Furthermore, the effects of SP were eliminated due to the stress relaxation because of a high temperature, resulting in a tensile residual stress value of 187 MPa.

For the SP + PIII 500 condition, the combination of SP and PIII treatments resulted in higher surface hardness and

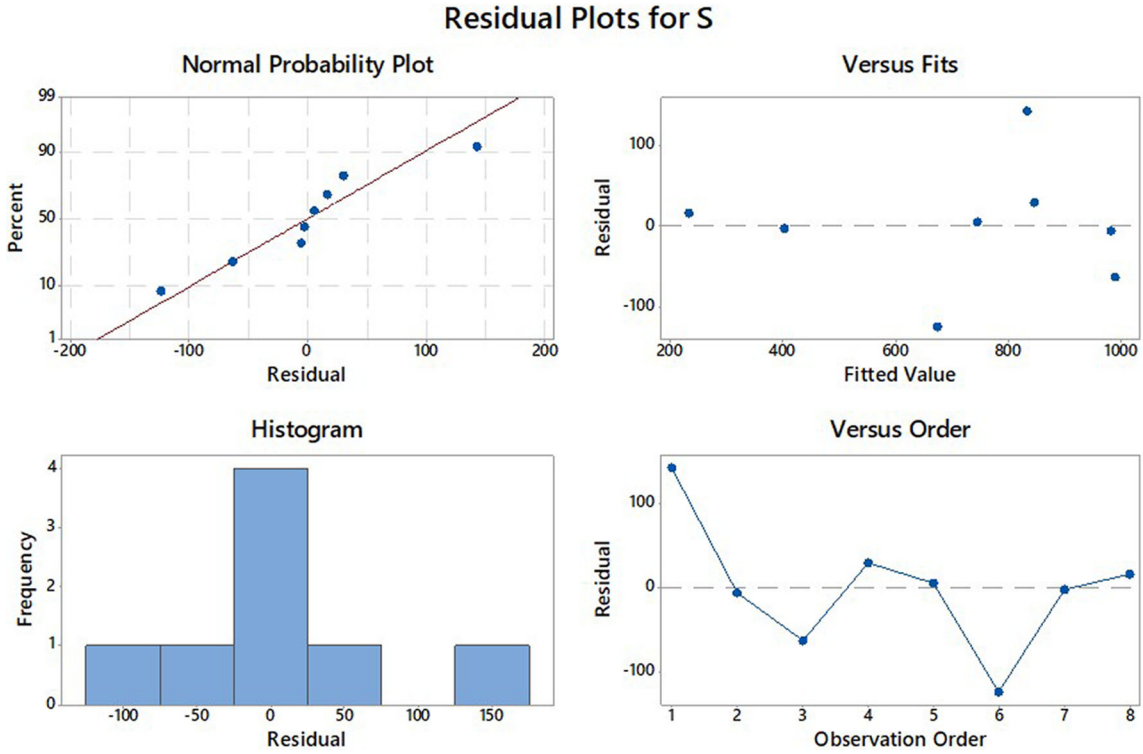

Fig. 16 Linear regression residual plots of the PIII 800 °C condition

enhanced compressive residual stress profile. Compared to the condition with only PIII, the formed ceramic coating during PIII treatments reduced fatigue resistance of the Ti-6Al-4V alloy (as explained above). In Table 2, the compressive residual stress value for the SP condition was − 119 MPa, while the PIII 500 condition resulted in a tensile residual stress of 189 MPa. A comparison of the PIII and SP combination treatment to the PIII treatment revealed that the fatigue strength increased in the high-cycle region based on the effects of compressive residual stress on the surface, which is produced by the SP process, reducing the effective applied stress and delaying crack nucleation. The residual stress values for PIII 500 and SP + PIII 500 conditions revealed that the residual stress value was significantly lower (23 MPa) for the SP + PIII 500 condition than that for PIII 500 (189 MPa). Therefore, the combination of SP and PIII at 500 °C was efficient to reduce the tensile residual stresses induced by the PIII process.

Therefore, the Ti-6Al-4V alloy with a lamellar microstructure (PIII 800) exhibited lower fatigue strength compared to the equiaxed microstructure. The SP process maintained the Ti-6Al-4V alloy's axial fatigue strength in the low-cycle fatigue regime based on compressive residual stress induced on the surface. However, in the high-cycle fatigue regime, the mean superficial roughness (5.88 μm) decreased the fatigue strength. PIII decreased the Ti-6Al-4V alloy's fatigue strength based on the induction of tensile residual stress on the surface. PIII and SP combined are particularly interesting at 500 °C, where the SP pretreatment decreased the tensile residual stress value from 189 to 23 MPa.

The fatigue fractures analysis, via SEM, and showed that crack nucleation occurred on the surface, for all experimental conditions.

Considering the presence of a ceramic layer (present in the conditions PIII 500, PIII 800, SP + PIII 500, and SP + PIII 800), Lynn et al. (Ref 60) demonstrated that once nucleation occurs on the coating surface, it propagates toward the substrate with no deflection and continues to propagate through the substrate according to the substrate's plastic deformation mechanisms. The authors also reported that increasing coating thickness leads to greater damage to the substrate via crack propagation (Ref 60). The differences in the fracture patterns of PIII-treated Ti-6Al-4V alloy at 500 (Fig. 8 and 9) and 800 °C (Fig. 11 and 12) revealed that, at 800 °C, the fracture had a brittle aspect and without plastic deformation, characteristics of catastrophic fractures. The difference between the elastic moduli of the ceramic coating (TiN) and the metal substrate (Ti-6Al-4V alloy) accelerated the crack initiation on the surface (Ref 61). During the propagation stage, such cracks encountered a region hardened by nitrogen diffusion and alpha phase stabilization, which has low resistance to propagation (Ref 61). Therefore, the combination of earlier crack initiation and low resistance to propagation reduced the fatigue life of the Ti-6Al-4V alloy, at PIII 800 condition.

One can see differences in the nucleation and propagation regions in Fig. 7 and 10. Figure 7 shows radial markers originating from the nucleation point, indicating that cracking occurred concentrically. Figure 10 shows a crack with an abrupt beginning and large size (Ref 62). The term ''abrupt'' refers to fast crack propagation rate, as was observed in the brittle aspect of the fracture with few dimples (i.e., plastic deformation) and more facets (i.e., cleavage). The term ''large size'' refers to the fact that the crack reached the metallic substrate with the size of the coating, which was approximately 8 μm (TiN + Ti_2N + N (α)). The cleavage surfaces presented by Fig. 11 are characteristic of dislocation slipping of the α basal plane, which results from the action of tensile stress normal to the slip and multiple crystallographic orientations. These different orientations result in heterogeneous deformation (Fig. 11c) with strong slip

activity in certain regions, leading to unfavorable cleavage of the basal plane (Ref 3, 63).

Regarding the dislocation structures and the change in the mechanical strength of the Ti-6Al-4V alloy with cyclic deformation, that is, with the number of cycles, the literature reports that titanium and Ti-10 V-2Fe−3A1 alloy exhibited cyclic softening (Ref 56, 64). In addition, the correlation between the limits established by Manson and Hirschberg (Ref 50) and stacking fault energy (SFE) values can define dislocations mobility and substructure stability after cyclic deformation. The SFE for titanium is approximately 300 mJ/m^2 (Ref 57). In this case, high SFE determines the ease of cross-slip occurrence. Cross-slip for metals with high SFE is relatively easy and activates dynamic recovery mechanisms. The softening phenomenon has been associated with dislocations annihilation enhanced by cross-slip in titanium and titanium alloys (Ref 56, 64). Figure 13(a) (bright field-TEM) and 13b (dark field-TEM) shows the dislocations structure of the specimen tested at 950 MPa. Tangles, dislocations in α/β interfaces and between the α grains, slip bands, heterogeneous distribution of dislocations, and low dislocations activity in β phase was observed. Cross-slip also leads to the slip bands and tangled dislocations in α grains. The formation of sliding bands during fatigue tests has also been reported on titanium and Ti-6242Si alloy (Ref 57, 64). There is strong evidence that dislocations have been nucleated from α/β interface and between α grains giving rise to tangles structure. As a result of recovery mechanisms, higher and lower dislocations density regions in the α phase are observed. This dislocations configuration offers less resistance to deformation. The strain-hardening exponent decreases with increasing SFE, which justifies $n = 0.097$ and σ_{UTS}/σ_{YS} ratio of 1.06 determined in this work. The behavior of two-phase alloys results mainly from the α-phase plasticity, usually softer than the β phase, as suggested by Luquiau (Ref 49) and Joseph (Ref 55).

Finally, the results, analyzed in light of the literature, indicated that the SP treatment increases the density of dislocations on surface, due to plastic deformation. This increase in dislocation density increases the local energy level, decreasing the nitrogen diffusion activation energy. Here, there is an indication of nitriding facilitation and the possibility of thermochemical treatments at lower temperatures, as in the case of the PIII 500 condition. The SP treatment can also increase (as it did) the surface roughness, which, when applied in a situation of cyclic deformation, acts as a multiplier of stress concentration sites on surface. The titanium alloy undergoes cyclic softening, as the dislocations present, especially in the alpha phase and in the basal slip system, tend to form substructures typical of the recovery process. The difference between the elastic modulus values of the Ti-6Al-4V alloy and the nitrided layer promoted the formation of cracks in the ceramic layer, reducing the cycles necessary for the crack nucleation. Under a low-cycle fatigue regime, the SP + PIII 500 condition was the one that less affected the Ti-6Al-4V fatigue performance. Here, this result indicates that the treatment performed at lower temperatures maintained the microstructure of the alloy and formed a thinner nitrided layers. During cyclic deformation, the crack has the size of the layer thickness (which is thinner than the one in PIII 800 condition), and, once formed, it propagates toward the center of the sample less easily than in the SP + PIII 800 condition, which has a higher residual tensile stress. This analysis indicates the need of new interactions of SP treatment with the PIII 500 implantation studies. In this way, the studies would be conducted varying the intensity of the peening, to generate higher levels of compressive residual stress; or even combining this treatment with other peening techniques to improve the surface finish and reduce roughness.

5. Conclusions

The present work investigated the tensile–tensile fatigue behavior at room temperature of the Ti-6Al-4V alloy subjected to plasma immersion ion implantation (PIII) at 500 °C and 800 °C, shot peening (SP) process and to the combination of both surface treatments. The analysis was based on the effects of applying shot peening treatment as a pre-treatment. Therefore, fatigue tests, residual stress measurements, microstructural analysis, scanning and transmission electron microscopies, surface roughness, fractography and statistics analysis were made. The main conclusions that can be drawn from this work are:

- The PIII treatment at 800 °C reduced the axial fatigue strength in both low- and high-cycle fatigue regimes, with a stronger effect in the high-cycle regime. The increase of the PIII treatment temperature reduced the Ti-6Al-4V alloy's axial fatigue strength because of thicker brittle layer generation on its surface. This promoting the participation of a thicker brittle compound in the fatigue process with an elastic modulus four times greater than Ti-6Al-4V alloy, which accelerated the crack nucleation on surface.
- The PIII treatment at 500 °C maintained about the same low-cycle fatigue strength (1035 MPa) compared to the Ti-6Al-4V alloy base material (1043 MPa). However, the fatigue strength significantly reduced at the high-cycle fatigue regime with the PIII treatment, where the crack nucleation is the factor that commands a longer or shorter fatigue life.
- The combination of SP and PIII treatments increased the Ti-6Al-4V alloy's fatigue strength in the high-cycle fatigue regime compared to only PIII treatment based on crack closure induced by compressive residual stresses.
- The introduction of SP as a pretreatment before the PIII treatment at 500 °C decreased the tensile residual stress value at the surface from 189 to 23 MPa, resulting in an improvement of the fatigue strength.
- Based on fractography analysis and investigation of the deformation mechanisms, the crack nucleation started on the surface, especially in the alpha phase regions and in the basal slip systems, where the increase in the dislocations density combined with the cyclic softening of the titanium locally reduced the mechanical strength of the Ti-6Al-4V alloy.

Acknowledgments

This work was supported by São Paulo Research Foundation (FAPESP), FAPESP grant numbers 2015/00331-2 and 2016/11731-4, and National Council for Scientific and Technological Development (CNPq), CNPQ grant number 303832/2014-2.

Conflict of interest

We wish to confirm that there are no known conflicts of interest associated with this publication and there has been no significant financial support for this work that could have influenced its outcome. All of the sources of funding for the work described in this publication are acknowledged. We confirm that we have given due consideration to the protection of intellectual property associated with this work and that there are no impediments to publication, including the timing of publication, with respect to intellectual property. In so doing we confirm that we have followed the regulations of our institutions concerning intellectual property. We understand that this Corresponding Author is the sole contact for the Editorial process. He/she is responsible for communicating with the other authors about progress, submissions of revisions and final approval of proofs.

References

1. D. Yonekura, J. Fujita, and K. Miki, Fatigue and Wear Properties of Ti-6Al-4V Alloy with Cr / CrN Multilayer Coating, *Surf. Coat. Technol.*, 2015, **275**, p 232–238
2. J. Su, X. Ji, J. Liu, J. Teng, F. Jiang, D. Fu, and H. Zhang, Revealing the Decomposition Mechanisms of Dislocations and Metastable α' Phase and their Effects on Mechanical Properties in a Ti-6Al-4V Alloy, *J. Mater. Sci. Technol.*, 2022, **107**, p 136–148
3. F. Bridier, P. Villechaise, and J. Mendez, Analysis of the Different Slip Systems Activated by Tension in a α/β Titanium Alloy in Relation with Local Crystallographic Orientation, *Acta Mater.*, 2005, **53**, p 555–567
4. L. Wanying, Effect of Different Heat Treatments on Microstructure and Mechanical Properties of Ti6Al4V Titanium Alloy, *Rare Metal. Mater. Eng.*, 2017, **46**, p 634–639
5. C. Tang, D. Liu, B. Tang, X. Zhang, L. Qin, and C. Liu, Influence of Plasma Molybdenizing and Shot Peening on Fretting Damage Behavior of Titanium Alloy, *Appl. Surf. Sci.*, 2016, **390**, p 946–958
6. M.Y. Costa, M.O. Cioffi, M.L. Venditti, and H.J. Voorwald, Fatigue Fracture Behavior of Ti-6Al-4V PVD Coated, *Proc Eng.*, 2010, **2**(1), p 1859–1864
7. V.M. de Oliveira, M.C. da Silva, C.G. Pinto, P.A. Suzuki, J.P. Machado, V.M. Chad, and M.J. Barboza, Short-Term Creep Properties of Ti-6Al-4V Alloy Subjected to Surface Plasma Carburizing Process, *J. Mater. Res. Technol.*, 2015, **4**(4), p 359–366
8. A. Zammit, M. Attard, P. Subramaniyan, S. Levin, L. Wagner, J. Cooper, L. Espitalier, and G. Cassar, Investigations on the Adhesion and Fatigue Characteristics of Hybrid Surface-Treated Titanium Alloy, *Surf. Coat. Technol.*, 2022, **431**, p 128002
9. S. Hémery, A. Nait-Ali, M. Guéguen, and P. Villechaise, Mechanical Study of Crystalline Orientation Distribution in Ti-6Al-4V: An Assessment of Micro-Texture Induced Load Partitioning, *Mater. Des.*, 2018, **137**, p 22–32
10. V. Saraiva, F. Bridier, and P. Bocher, Predicting the Effects of Material Properties Gradient and Residual Stresses on the Bending Fatigue Strength of Induction Hardened Aeronautical Gears, *I. J. Fatigue*, 2016, **85**, p 70–84
11. C.B. Mello, M. Ueda, M.M. Silva, H. Reuther, L. Pichon, and C.M. Lepienski, Tribological Effects of Plasma Immersion ion Implantation Heating Treatments on Ti-6Al-4V Alloy, *Wear*, 2009, **267**, p 867–873
12. T.A. Minto, V.M.C.A. Oliveira, and H.J.C. Voorwald, Plasma Immersion Ion Implantation: Influence on the Rotating Bending Fatigue Strength of AA 7050-T7451 Aluminum Alloy Int, *J. Fatigue*, 2017, **103**, p 17–27
13. H. Liu, B. Tang, L. Wang, X. Wang, and B. Jiang, Fatigue Life and Mechanical Behaviors of Bearing Steel by Nitrogen Plasma Immersion Ion Implantation, *Surf. Coat. Technol.*, 2007, **201**, p 5273–5277
14. F. Abdi and H. Savaloni, Surface nanostructure modification of Al substrates by N + ion implantation and their corrosion inhibition Trans, *Nonferrous Met. Soc. China*, 2016, **27**, p 701–710
15. Y.C. Bastos, M.F. Fernandes, V.M. de Oliveira Velloso, T.A. Minto, and H.J. Voorwald, Plasma Immersion Ion Implantation and Shot Peening Influence on the Fatigue Strength of AA 7050-T7451 Aluminum Alloy, *Eng. Res. Express.*, 2020, **2**(1), p 015015
16. L. Wang, L. Zhou, L. Liu, W. He, X. Pan, X. Nie, and S. Luo, Fatigue Strength Improvement in Ti-6Al-4V Subjected to Foreign Object Damage by Combined Treatment of Laser Shock Peening and Shot Peening, *Int. J. Fatigue.*, 2022, **155**, p 106581
17. H. Xiao, X. Liu, Q. Lu, T. Hu, Y. Hong, C. Li, R. Zhong, and W. Chen, Promoted Low-Temeperature Plasma Nitriding for Improving Wear Performance of Arc-Deposited Ceramic Coatings on Ti6Al4V Alloy Via Shot Peening Pretreatment, *J. Mater. Res. Technol.*, 2022, **19**, p 2981–2990
18. S.Q. Wang, W.Y. Li, Y. Zhou, X. Li, and D.L. Chen, Tensile and Fatigue Behavior of Electron Beam Welded Dissimilar Joints of Ti-6Al-4V and IMI834 Titanium Alloys, *Mater. Sci. Eng. A.*, 2016, **649**, p 146–152
19. M.F. Fernandes, M.A. Torres, M.D. Fonseca, and C.A. Baptista, Investigation of Residual Stress, Stress Relaxation and Work Hardening Effects Induced by Shot Peening on the Fatigue Life of AA 6005-T6 Aluminum Alloy, *Mater. Res. Express.*, 2020, **6**(12), p 1265i2
20. S.R. Hosseini and A. Ahmadi, Evaluation of the Effects of Plasma Nitriding Temperature and Time on the Characterisation of Ti 6Al 4V Alloy, *Vacuum*, 2013, **87**, p 30–39
21. D. She, W. Yue, Z. Fu, C. Wang, X. Yang, and J. Liu, Effects of Nitriding Temperature on Microstructures and Vacuum Tribological Properties of Plasma-Nitrided Titanium, *Surf. Coat. Technol.*, 2015, **264**, p 32–40
22. S. Li, X. Zhao, Y. An, W. Deng, G. Hou, E. Hao et al., Effect of Deposition Temperature on the Mechanical, Corrosive and Tribological Properties of Mullite Coatings, *Ceram. Int.*, 2018, **44**, p 6719–6729
23. T. Morita, K. Asakura, and C. Kagaya, Effect of Combination Treatment on Wear Resistance and Strength of Ti-6Al-4V Alloy, *Mater. Sci. Eng. A*, 2014, **618**, p 438–446
24. K. Farokhzadeh and A. Edrisy, Fatigue Improvement in Low Temperature Plasma Nitrided Ti-6Al-4V Alloy, *Mater. Sci. Eng. A.*, 2015, **620**, p 435–444
25. D. Manova, S. Mändl, H. Neumann, and B. Rauschenbach, Wear Behaviour of Martensitic Stainless Steel After PIII Surface Treatment, *Surf. Coat. Technol.*, 2005, **200**, p 137–140
26. M. Ueda, M.M. Silva, C. Otani, H. Reuther, M. Yatsuzuka, and C.M. Lepienski, Improvement of Tribological Properties of Ti6Al4V by Nitrogen Plasma Immersion Ion Implantation, *Surf. Coat. Technol.*, 2003, **169**, p 408–410
27. J.H. Chang, S. Wang, H. Pan, M.F. Wu, D.K. Shiau, and H.H. Huang, Nitrogen Plasma Immersion Ion Implantation Treatment of Ti6Al7Nb Alloy for Bone-Implant Applications: Enhanced in vitro Biological Responses and in vivo Initial Bone-Implant Contact, *Surf. Coat. Technol.*, 2021, **405**, p 126551
28. A. Shanaghi and P.K. Chu, Enhancement of Mechanical Properties and Corrosion Resistance of NiTi Alloy by Carbon Plasma Immersion Ion Implantation, *Surf. Coat. Technol.*, 2018, **365**, p 52–57
29. B.C.E. Kurelo, G.B. Souza, F.C. Serbena, W.R. Oliveira, C.E.B. Marino, and L.A. Taminato, Performance of Nitrogen Ion-Implanted Supermartensitic Stainless Steel in Chlorine- and Hydrogen-Rich Environments, *Surf. Coat. Technol.*, 2018, **351**, p 29–41
30. V.M.C.A. Oliveira, M.O.H. Cioffi, M.J.R. Barboza, R. Landers, B. Schmitt, D.C.A.R. Tapia, and H.J.C. Voorwald, Plasma Immersion Ion Implantation (PIII) Influence on Ti-6Al-4V Alloy: Frequency Effect, *Int J Fatigue*, 2017, **109**, p 157–165
31. V. Velloso, L. Nozaki, D. Tapia, M.O. Cioffi, R. Oliveira, M. Barboza et al., Fatigue Behavior of Ti-6Al-4V Alloy Modified by Plasma Immersion Ion Implantation: Temperature Effect, *MATEC Web. Conf.*, 2018, **165**, p 2–7
32. Q. Yang, W. Zhou, Z. Niu, X. Zheng, Q. Wang, X. Fu et al., Effect of Different Surface Asperities and Surface Hardness Induced by Shot-Peening on the Fretting Wear Behavior of Ti-6Al-4V, *Surf. Coat. Technol.*, 2018, **349**, p 1098–1106
33. Z. Xu, J. Dunleavey, M. Antar, R. Hood, S.L. Soo, G. Kucukturk et al., The Influence of Shot Peening on the Fatigue Response of Ti-6Al-4V Surfaces Subject to Different Machining Processes, *Int. J. Fatigue*, 2018, **111**, p 196–207
34. H.J. Voorwald, L.F. dos Santos Vieira, V.M. de Oliveira Velloso, M.F. Fernandes, and M.O. Cioffi, Investigation of HVOF-Sprayed WC-and NiCr-Based Coatings to Improve Corrosion and Wear Performance of High-Strength Steel, *J. Braz. Soc. Mech. Sci. Eng.*, 2022, **44**(3), p 96

35. M. Santos, J. Rodrigo, M.F. Fernandes, V.M.O. Velloso, and H.J.C. Voorwald, Fatigue Analysis of Threaded Components with Cd and Zn-Ni Anticorrosive Coatings, *Metals*, 2021, **11**, p 1455
36. ASTM F136-13, Standard Specification for Wrought Titanium-6Aluminum-4Vanadium ELI (Extra Low Interstitial) Alloy for Surgical Implant Applications (UNS R56401), ASTM International, West Conshohocken, PA, (2013)
37. SAE AMS B Finishes Processes and Fluids Committee, SAE Standard AMS 2430—Shot Peening, Automatic (2009)
38. M. Thomas, T. Lindley, D. Rugg, and M. Jackson, The Effect of Shot Peening on the Microstructure and Properties of a Near-Alpha Titanium Alloy Following High Temperature Exposure, *Acta Mater*, 2012, **60**, p 5040–5048
39. B.K.C. Ganesh, W. Sha, N. Ramanaiah, and A. Krishnaiah, Effect of Shot Peening on Sliding Wear and Tensile Behavior of Titanium Implant Alloys, *Mater. Des.*, 2014, **56**, p 480–486
40. S. Bagherifard, Enhancing the Structural Performance of Lightweight Metals by Shot Peening, *Adv. Eng. Mater.*, 2019, **21**, p 1801140
41. R.M. Oliveira, J.A.N. Gonçalves, M. Ueda, J.O. Rossi, and P.N. Rizzo, A New High-Temperature Plasma Immersion Ion Implantation System with Electron Heating, *Surf. Coat. Technol.*, 2010, **204**, p 3009–3012
42. X. Yang and R. Liu, Machining Titanium and its Alloys, *Mach. Sci. Technol.*, 1999, **3**, p 107–139
43. D. Setti, M.K. Sinha, S. Ghosh, and P.V. Rao, Performance Evaluation of Ti-6Al-4V Grinding Using Chip Formation and Coefficient of Friction Under the Influence of Nanofluids, *I. J. Mach. Tools Manuf.*, 2015, **88**, p 237–248
44. International A. ASTM E466-15 Standard Practice for Conducting Force Controlled Constant Amplitude Axial Fatigue Tests of Metallic Materials. West Conshohocken (2015)
45. ASTM. ASTM E739 - Standard Practice for Statistical Analysis of Linear or Linearized Stress-Life (S-N) and Strain-Life (ε-N) Fatigue Data Statistical Analysis of Fatigue Data, (2015)
46. ISO 12107:2012 Metallic materials — Fatigue testing — Statistical Planning and Analysis of Data. Geneva, Switzerland, (2003)
47. S. Jagatheeshkumar, M. Raguraman, S.P. AVS, B.K. Nagesha, and U. Chandrasekhar, Study of Residual Stresses and Distortions from the Ti6Al4V Based Thin-Walled Geometries Built Using LPBF Process, *Def. Technol.*, 2023 https://doi.org/10.1016/j.dt.2023.01.002
48. H. Zhang, Z. Cai, J. Chi, R. Sun, Z. Che, H. Zhang, and W. Guo, Fatigue Crack Growth in Residual Stress Fields of Laser Shock Peened Ti6Al4V Titanium Alloy, *J All Com*, 2021, **887**, p 161427
49. M.V. Nataraj and S. Swaroop, Effects of Power Density on Residual Stress and Microstructural Behavior of Ti-2.5 Cu Alloy by Laser Shock Peening without Coating, *Vacuum*, 2023, **213**, p 112078
50. Manson, SS and M. Hirschberg MH, Fatigue: An Interdisciplinary Approach, Syracuse University Press, Syracuse, NY, 1964, p. 133
51. D. Munz, Workhardening, Slip Band Formation and Crack Initiation During Fatigue of Titanium, *Eng. Fract. Mech.*, 1973, **5**, p 353–364
52. H. Knobbe, P. Köster, H.J. Christ, C.P. Fritzen, and M. Riedler, Initiation and Propagation of Short Fatigue Cracks in Forged Ti6Al4V, *Proc. Eng.*, 2010, **2**, p 931–940
53. Y. Ma, Q. Xue, H. Wang, S. Huang, J. Qiu, X. Feng, J. Lei, and R. Yang, Deformation Twinning in Fatigue Crack Tip Plastic Zone of Ti-6Al-4V Alloy with Widmanstatten Microstructure, *Mater. Charact.*, 2017, **132**, p 338–347
54. J. Qiu, X. Feng, Y. Ma, J. Lei, Y. Liu, A. Huang et al., Fatigue Crack Growth Behavior of Beta-Annealed Ti-6Al-2Sn-4Zr-xMo (x = 2, 4 and 6) Alloys: Influence of Microstructure and Stress Ratio, *Int J Fatigue*, 2016, **83**, p 150–160
55. S. Griza, C.E.C. de Andrade, W.W. Batista, E.K. Tentardini, and T.R. Strohaecker, Case Study of Ti6Al4V Pedicle Screw Failures Due to Geometric and Microstructural Aspects, *Eng. Fail. Anal.*, 2012, **25**, p 133–143
56. H. Shibata, K. Tokaji, T. Ogawa, and C. Hori, The Effect of Gas Nitriding on Fatigue Behaviour in Titanium Alloys, *Int. J. Fatigue*, 1994, **16**, p 370–376
57. W.J. Evans, Optimising Mechanical Properties in alpha+beta Titanium Alloys, *Mater. Sci. Eng. A*, 2002, **243**, p 89–96
58. A. Soltani-Tehrani, M. Habibnejad-Korayem, S. Shao, M. Haghshenas, and N. Samsaei, Ti-6Al-4V Powder Characteristics in Laser Powder Bed Fusion: The Effect on Tensile and Fatigue Behavior, *Add. Manuf.*, 2022, **51**, p 102584
59. Q. Yang, W. Zhou, Z. Niu, X. Zheng, Q. Wang, X. Fu et al., Effect of Different Surface Asperities and Surface Hardness Induced by Shot Peening on the Fretting Wear Behavior of Ti-6Al-4V, *Surf. Coat. Technol.*, 2018, **349**, p 1098–1106
60. Q. Yang, W. Zhou, Y. Zhong, X. Zhang, X. Fu, G. Chen et al., Effect of Shot-Peening on the Fretting Wear and Crack Initiation Behavior of Ti-6Al-4V Dovetail Joint Specimens, *Int. J. Fatigue*, 2018, **107**, p 83–95
61. H. Kovaci, I. Hacisalihoglu, A.F. Yetim, and A. Çelik, Effects of Shot Peening Pre-Treatment and Plasma Nitriding Parameters on the Structural, Mechanical and Tribological Properties of AISI4140 Low-Alloy Steel, *Surf. Coat. Technol.*, 2019, **358**, p 256–265
62. A.F. Yetim, H. Kovaci, Y. Uzun, H. Tekdir, and A. Çelik, A Comprehensive Study on the Fatigue Properties of Duplex Surface Treated Ti6Al4V by Plasma Nitriding and DLC Coating, *Surf. Coat. Technol.*, 2023, **458**, p 129367
63. K. Lynn and D.L. DuQuesnay, Hydroxyapatite-coated Ti-6Al-4V: Part 1: The Effect of Coating Thickness on Mechanical Fatigue Behaviour, *Biomater*, 2002, **23**, p 1937–1946
64. C.X. Li, D. Horspool, and H. Dong, Effect of Ceramic Conversion Surface Treatment on Fatigue Properties of Ti6Al4V Alloy, *Int. J. Fatigue*, 2007, **29**, p 2273–2280
65. D. Luquiau, X. Feaugas, and M. Clavel, Cyclic softening of the Ti-10V-2Fe-3Al Titanium Alloy, *Mater. Sci. Eng., A*, 1997, **224**, p 146–156
66. R. Salloom, R. Banerjee, and S.G. Srinivasan, Effect of β-Stabilizer Elements on Stacking Faults Energies and Ductility of α-Titanium Using First-Principles Calculations, *J. Appl. Phys.*, 2016, **17**, p 120
67. S. Joseph, T.C. Lindley, and D. Dye, Dislocation Interactions and Crack Nucleation in a Fatigued Near-Alpha Titanium Alloy, *Int. J. Plast.*, 2018, **110**, p 38–56